INVITED PAPER *Special Section on Microwave and Millimeter-Wave Technologies*

A 24–30 GHz Power Amplifier with >20-dBm Psat and <0.1-dB AM-AM Distortion for 5G Applications in 130-nm SiGe BiCMOS

Chihiro KAMIDAKI†a), ***Member***, **Yuma OKUYAMA**†, **Tatsuo KUBO**†, **Wooram LEE**††, **Caglar OZDAG**††, **Bodhisatwa SADHU**††, ***Nonmembers***, **Yo YAMAGUCHI**†, ***Senior Member***, ***and*** **Ning GUAN**†, ***Member***

SUMMARY This paper presents a power amplifier (PA) designed as a part of a transceiver front-end fabricated in 130-nm SiGe BiCMOS. The PA shares its output antenna port with a low noise amplifier using a low-loss transmission/reception switch. The output matching network of the PA is designed to provide high output power, low AM-AM distortion, and uniform performance over frequencies in the range of 24.25–29.5 GHz. Measurements of the front-end in TX mode demonstrate peak S_{21} of 30.3 dB at 26.7 GHz, S_{21} 3-dB bandwidth of 9.8 GHz from 22.2 to 32.0 GHz, and saturated output power (Psat) above 20 dBm with power-added efficiency (PAE) above 22% from 24 to 30 GHz. For a 64-QAM 400 MHz bandwidth orthogonal frequency division multiplexing (OFDM) signal, −25 dBc error vector magnitude (EVM) is measured at an average output power of 12.3 dBm and average PAE of 8.8%. The PA achieves a competitive ITRS FoM of 92.9.

key words: *5G, mm-wave, power amplifier, SiGe BiCMOS tecnology, EVM, ACLR, PAE, AM-AM, AM-PM*

1. Introduction

The 5th generation of mobile technology (5G) has been launched and is now being rapidly adopted all over the world [1]–[5]. Applying mm-wave is a key technology for the 5G networks and is also very challenging [6]–[8]. Several mm-wave 5G phased array antenna modules (PAAM) have been reported [9]–[21]. The authors have presented PAAM consisting of multiple ICs of beamforming IC and frequency conversion IC in multilayer antenna-in-package, containing passive components such as liquid crystal polymer (LCP) bandpass filters [22]–[26]. For Si-based phased arrays, research has focused on how to improve the effective isotropically radiated power (EIRP), as this can contribute to covering larger areas for base stations. While the EIRP can be improved by increasing the number of antenna elements, this comes at the expense of antenna array area and cost. Alternatively, the EIRP can be improved by increasing the output power of the power amplifier (PA). It is also very important to improve the efficiency at the same time so as to avoid the undesirable side-effect of requiring a complex thermal solution. Moreover, PA designs for 5G applications utilizing multi-carrier higher-order modulations are subject to strict linearity requirements, i.e., low AM-AM and AM-PM [27]. Due to the high peak-to-average ratio (PAPR) and sensitivity to distortion of the high-order quadrature amplitude modulation (e.g., 64-QAM) signals, the PA needs to be operated at considerable back-off, which leads to efficiency degradation [28]. Lastly, a broadband PA architecture is desired to cover multiple bands of 5G NR.

The performance of the PA has a significant impact on wireless communications, so various proposals have been made to meet the required specifications. For example, techniques using GaN and GaAs have been reported to show high output power for mm-wave applications [29], [30]. Nevertheless, since 5G mm-wave base stations perform beamforming using a large number of PAs, they should be inexpensive, mass-producible and easy-to-integrate with phase controller. For this reason, SiGe BiCMOS and CMOS PAs have been proposed as preferred for this application [27], [28], [31]–[33]. In addition, while circuit topologies such as Doherty and outphasing are highly efficient as described in [34], [35], they tend to be large in size, so miniaturised PAs are preferable.

The authors have previously reported a transformer-coupled 2-stage differential PA that meets the above-mentioned requirements of the 5G mm-wave applications [36]. In this paper, we discuss the PA in detail.

The proposed PA shares its antenna port with a co-designed low noise amplifier (LNA) and a transmission/reception switch (TRX SW) that comprise a transceiver front-end. The output matching network (OMN) of the PA includes the off-state LNA and the on-state TRX SW, and is optimized using load pull simulations to obtain the desired high output power and uniform frequency response. The LNA and TRX SW topologies are similar to the design reported in [25] and [26]. Our PA demonstrates a competitive output power, a linearity and efficiency from 24 to 30 GHz that cover multiple 5G NR FR2 bands, and a competitive Figure of Merit (FoM) defined by the International Technology Roadmap for Semiconductors (ITRS) continuous-wave (CW) test [37]. Modulation signal tests of the PA also demonstrate a low error vector magnitude (EVM) performance at a high average output power.

Manuscript received January 27, 2023.
Manuscript revised March 6, 2023.
Manuscript publicized May 12, 2023.

[†] The authors are with the Electronic Technologies R&D Center, Fujikura Ltd., Sakura-shi, 285–8550 Japan.

[††] The authors are with IBM Thomas J. Watson Research Center, Yorktown Heights, NY, USA.

a) E-mail: chihiro.kamidaki@jp.fujikura.com

DOI: 10.1587/transele.2023MMI0003

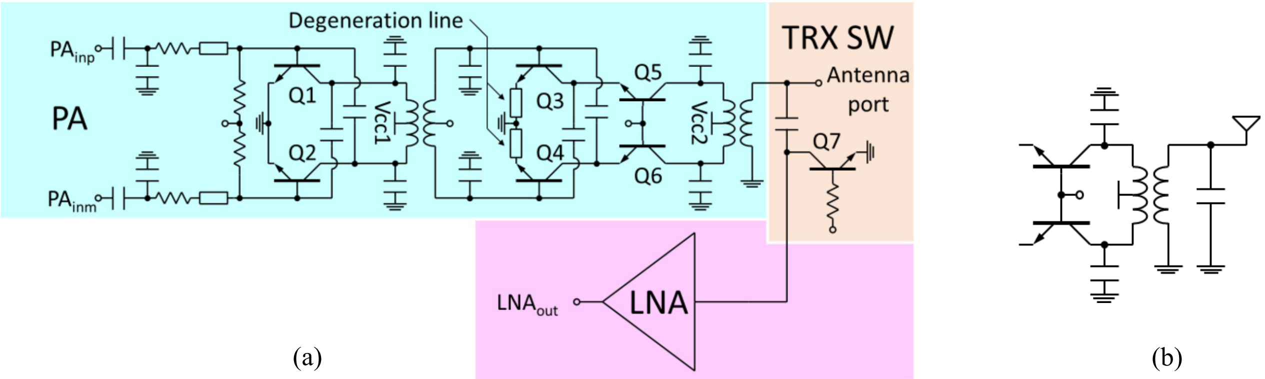

(a) (b)

Fig. 1 (a) Schematic of the proposed PA comprising a front-end. (b) Equivalent OMN circuit of the proposal PA in TX mode.

2. Circuit Design

2.1 Circuit Configuration

Figure 1 (a) shows the schematic of the proposed front-end consisting of the PA, LNA, and TRX SW. The first and second stages of the PA use a differential common-emitter-amplifier topology (Q1-2) and a differential cascode amplifier topology (Q3-4-5-6), respectively. They are coupled by an interstage matching network applying a doubly tuned transformer network for wide bandwidth [38]. The power supply of $\mathrm{Vcc}_1 = 1.5\,\mathrm{V}$ for the first stage and the base bias of the common-emitter (CE) transistors for the second stage are provided through the center taps of the primary and secondary windings of the transformer. The base of the CE transistors for both stages (Q1-2 and Q3-4, respectively) are biased by current mirror circuit controlled by an external current source. The base bias voltage of the common-base (CB) transistors Q5-6 is set by an integrated regulator.

The transistor Q7 switches the RF signal path based on TX or RX mode. In TX mode, it turns on and the OMN of the PA configures the transformer-coupled doubly tuned circuit as shown in Fig. 1 (b). The OMN is simultaneously exploited for differential to single-ended conversion for connection to an external antenna, which is typically single-ended. The power supply of $\mathrm{Vcc}_2 = 2.7\,\mathrm{V}$ for the second stage is provided through the center taps of the primary winding of the balun.

The second stage connects the degeneration transmission lines to the CE transistors Q3-4. They provide negative feedback that is expected to reduce the distortion and degrade gain. The length of the lines is selected based on the trade-off between AM-AM distortion improvement and of PAE degradation.

2.2 Circuit Stability

Although a PA requires not only output power but also high gain, this increases the possibility of oscillation. To improve stability, both the stages utilize capacitive neutralization between the base and collector terminals of the CE transistors to cancel out the Miller capacitance. The CB transistors can reduce the Miller effect, so utilizing a cascode configuration improves the stability of the second stage [39]. However, since the degeneration lines in the second stage are placed away from the transformers in layout, we had to lengthen the transmission lines to the base of transistors Q3-4 and to neutralizer capacitors, which increases the inductance and create more instability and mismatching of neutralizing capacitance. The thick metal layers of the interconnections of the second stage are therefore electromagnetically (EM) modeled and simulated as shown in Fig. 2.

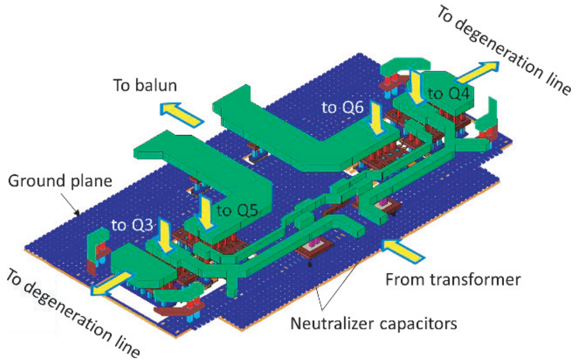

Fig. 2 EM model of thick metal interconnection of the second stage.

An unintentional coupling between inductors/transformers can also degrade the stability. To verify this by using the K-factor, the OMN balun and the interstage transformer are simultaneously EM simulated as shown in Fig. 3 (a) and subsequently integrated into a circuit simulation together with EM models of the interconnections of the second stage. Figure 3 (b) shows the K-factors of the PA under an unstable PVT condition (low temperature of −40 °C, +5% higher supply voltage, and fast BJT process corner) with the above EM models. For comparison, the K-factor without coupling between the transformer and balun is also shown. Although the coupling leads to less stability, the minimum value is still sufficiently larger than 1.

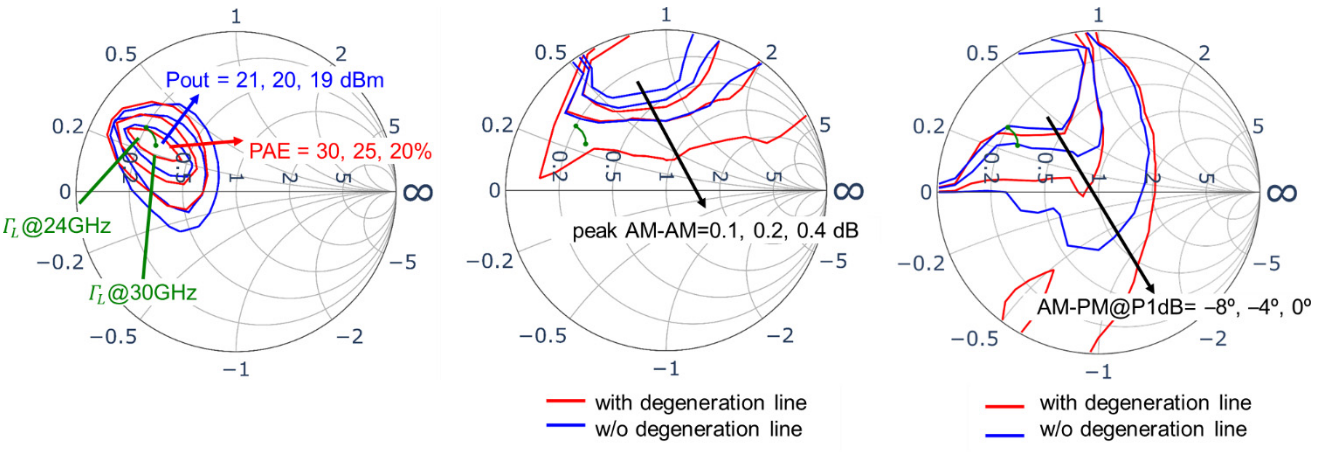

(a) (b) (c)

Fig. 4 (a) Load-pull simulation of PA with input signal of 0 dBm at 28 GHz. (b) Peak AM-AM contour across load impedance at 28 GHz. (c) AM-PM at P1dB contour across load impedance.

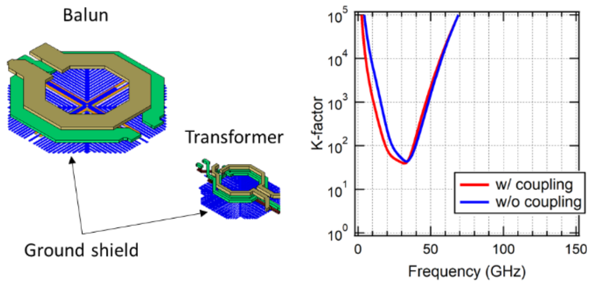

(a) (b)

Fig. 3 (a) EM model of the interstage transformer and OMN balun. (b) Comparison of simulated K-factor of the PA with and without coupling between the transformer and balun.

2.3 Load Pull Simulations

Figure 4 (a) shows the simulated load-pull contours for output power (Pout; blue) and power-added efficiency (PAE; red) with an input power (Pin) of 0 dBm at 28 GHz. In the simulation, a port with variable reflection coefficient and supply chokes are connected to collector of Q5-6, and both the PA stages are biased in class-AB. According to the simulated results of Pout, the TX-mode saturated output power (Psat) of the proposed PA is expected to be 20 dBm by an estimated 1-dB loss of the OMN, as discussed in next subsection. The PAE contours reach 30% efficiency and show good agreement with the Pout contours; as a result, we design the input impedance of the OMN of the PA with an antenna port (50 Ω) by targeting the center of the efficiency and Pout contours.

Figure 4 (b) shows the simulated peak AM-AM contours derived from the simulation of the PA with the power-swept input signal and variable impedance of the load at 28 GHz. Here, AM-AM is defined as the gain difference from a small signal gain, and peak AM-AM is defined as the difference between a small signal gain and the maximum large-signal gain. The figure shows the impedance range where AM-AM distortion suppression is improved by using the transmission line degeneration (red vs. blue). The length of the transmission line is set so that the AM-AM peak value is in the range of 0.2 to 0.4 dB while maintaining a high output 1 dB compression point (oP1dB).

Figure 4 (c) shows the simulated AM-PM at P1dB contours across load impedances at 28 GHz obtained in the same simulation as for Fig. 4 (b). In this work, AM-PM is defined as the phase difference from phase at a small signal, and we utilize AM-PM at P1dB to assess the phase variation at the point where the largest variation is shown in the linear region. The load impedance range where PA exhibits a low AM-PM at P1dB is shifted to a high impedance range overall by the degeneration transmission line, which is not a favorable transition for the OMN with matching at low impedance.

To compensate for the AM-PM degradation, we adjusted the size of the CB transistors Q5-6. Figure 5 (a) and (b) show the simulated AM-PM and AM-AM response of the PA equipped with CB transistors of different sizes. When the CB transistor is 20% larger than the CE transistor, the peak AM-AM is actually a bit higher, but oP1dB is improved, while maintaining the size of the CE transistors which affects the DC current consumption. At the same time, the peak AM-PM value is slightly higher, but the AM-PM response is extended to higher output power. As described in [25], the OMN contains a common impedance due to the capacitor connected in parallel in TX mode and in series in RX mode. The larger CB transistors increase the capacitance connected in parallel to the common impedance in RX mode, making it difficult for the LNA matching network to absorb the load of the switched-off PA. Therefore the size is selected based on trade-off between improvement of AM-PM distortion and impedance matching of the LNA.

Guided by these contour simulations as a basis, we set the optimized impedance of the PA OMN (Γ_L; shown in Fig. 6 (a)) from 24 to 30 GHz, as shown in green in Fig. 4.

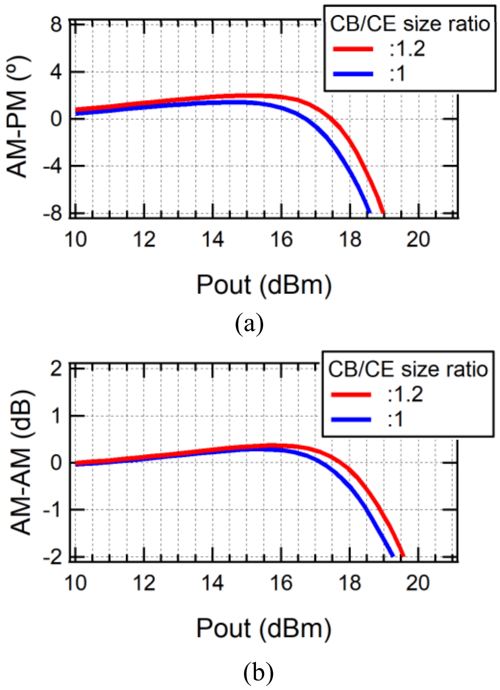

(a)

(b)

Fig. 5 Simulated AM-AM/AM-PM response of PA with the CB transistors of the same size or 20% larger than the CE transistors. (a) AM-PM response. (b) AM-AM response.

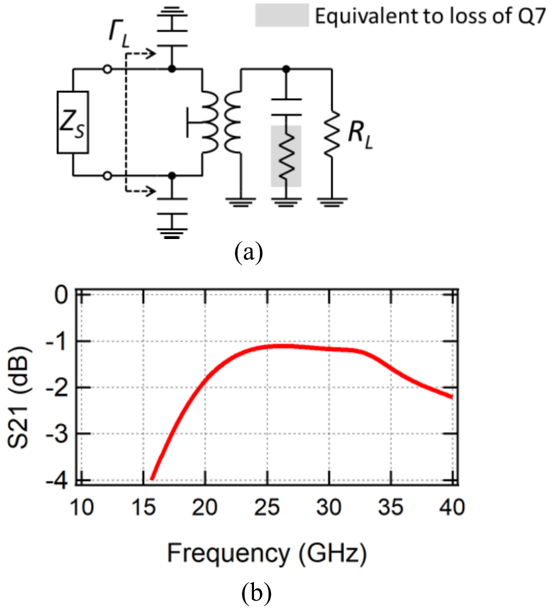

(a)

(b)

Fig. 6 (a) Equivalent OMN circuit in which the impedance of the output transistor is replaced by Z_s. (b) Insertion loss of OMN seen from Z_s.

Assuming a port with a source impedance Z_S equal to the conjugate of Γ_L, we can calculate the insertion loss of the OMN as shown in Fig. 6 (b). The OMN shows extremely flat response with less than 0.1 dB variation from 24 to 30 GHz. Despite the inclusion of a transistor switch which introduces a loss as shown in Fig. 6 (a), the OMN has a low insertion loss of approximately 1.2 dB or less, assuming a load impedance R_L of 50 Ω.

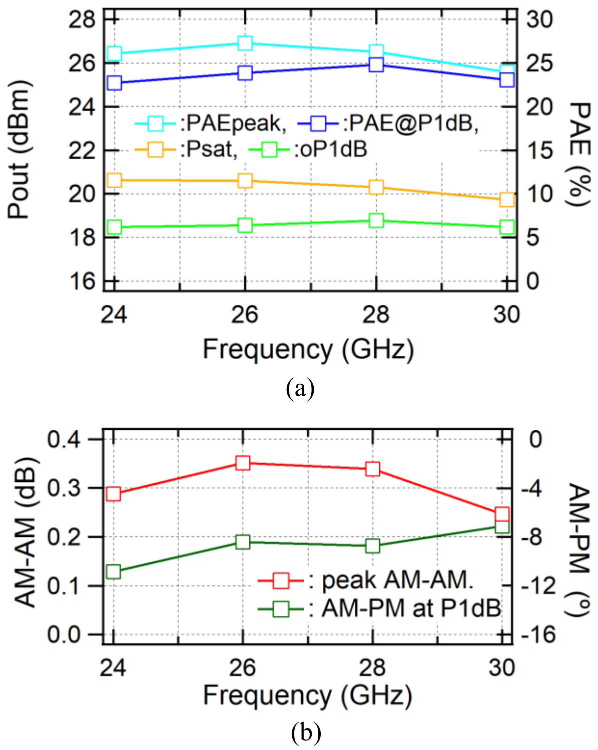

(a)

(b)

Fig. 7 Simulated performances of the proposal PA at different frequencies. (a) Psat, oP1dB, PAE peak, and PAE at P1dB. (b) Peak AM-AM and AM-PM at P1dB.

Figure 7 shows the simulated performance of the proposed PA, Psat, oP1dB, PAE peak, PAE at P1dB, peak AM-AM, and AM-PM at P1dB at the same frequencies. As expected from the power contour, Psat exhibits approximately 20 dBm and good flatness from 24 to 30 GHz. Also oP1dB is kept above 18 dBm in the same frequency range. After making adjustments based on the degeneration lines, the peak AM-AM is suppressed to less than 0.4 dB, while AM-PM at P1dB deteriorates as the frequency get lower, as expected from load-pull simulations.

3. Measurement Results

The front-end circuit is fabricated in 130-nm SiGe BiCMOS technology. The PA occupies a $0.63 \times 0.34\,\text{mm}^2$ active area, as shown in the micrograph in Fig. 8. A DC bias/supply currents/voltages to each of the stages are provided from pads on the top and bottom sides. Measurements are taken at room temperature and the first and second stages are biased to have collector current densities of $5.6\,\text{mA}/\mu\text{m}^2$ and $2.1\,\text{mA}/\mu\text{m}^2$, respectively, at the DC operating point.

3.1 S-Parameter Measurement

TX-mode small-signal S-parameters are measured using a Keysight N5247A Vector Network Analyzer. Figure 9 compares the measured and simulated S-parameters. The TX-mode S_{21} of the PA demonstrates a peak gain of 30.3 dB at

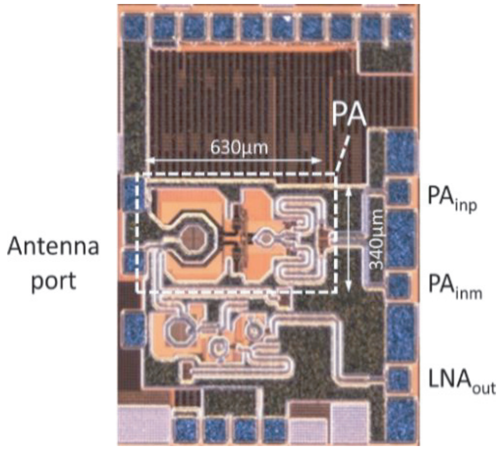

Fig. 8 Micrograph of implemented front-end circuit fabricated in 130-nm SiGe BiCMOS process. The PA active area is $0.63 \times 0.34\,\mathrm{mm}^2$.

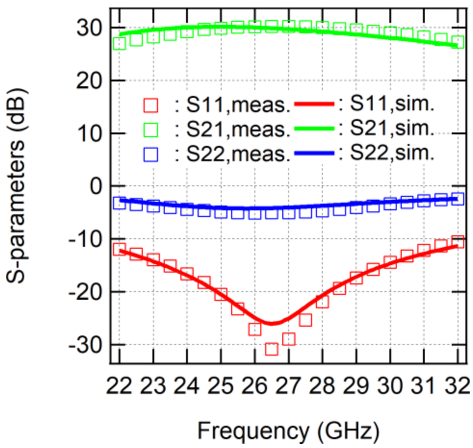

Fig. 9 Comparison of measured and simulated S-parameters of PA in TX mode.

26.7 GHz, $BW_{-3\mathrm{dB}}$ of 9.8 GHz from 22.2 to 32.0 GHz, and S_{11} of < -10 dB from 20.6 to 32.2 GHz. The $S_{22} < -3$ dB from 22.6 to 30.0 GHz, since the OMN has been optimized for power match using load-pull simulations. The largest difference between the simulated and measured S_{21} values from 24 to 30 GHz is 0.96 dB at 30 GHz. Thanks to the detailed parasitic and EM modeling, the measured frequency response shows good matching with the simulations.

3.2 CW Large Signal Measurement

Figures 10 and 11 compare the measured and simulated CW large-signal response of Pout and PAE, respectively, at 24, 26, 28 and 30 GHz. The input signal is generated from an E8257 Signal Generator and the output power is monitored using a Keysight N8487A Power Sensor. Overall, the measurements are in good agreement with the simulations. Figure 12 shows comparison of the measured and simulated AM-PM and AM-AM responses at 28 GHz. The phase of the PA output is measured by N5247. The measured and simulated AM-PM at P1dB is −8.0° and −8.7°, respectively,

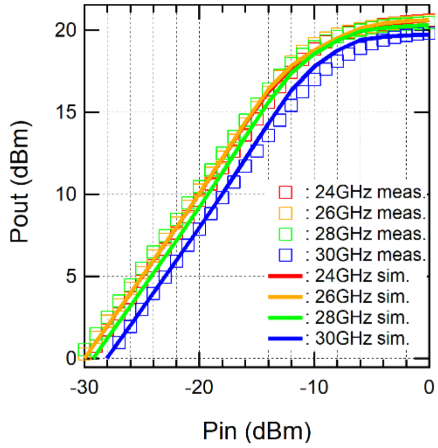

Fig. 10 Pout of PA by CW large-signal measurement and simulation.

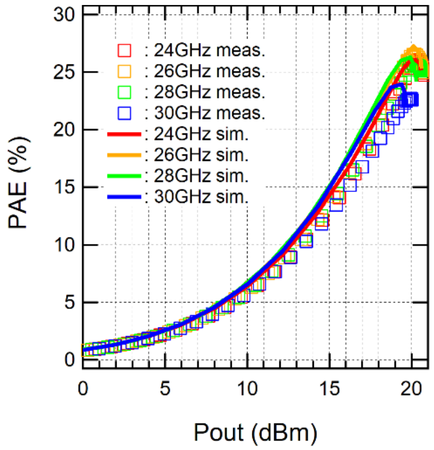

Fig. 11 PAE of PA by CW large-signal measurement and simulation.

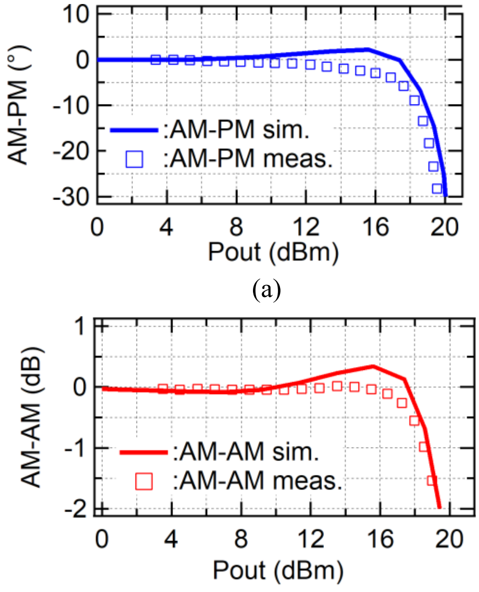

(a)

(b)

Fig. 12 Comparison of measured and simulated (a) AM-PM response and (b) AM-AM response at 28 GHz.

Table 1 Summary of PA performances.

	This Work				[27] ISSCC 2018	[31] RFIC 2021	[28] JSSC 2016	[32] IMS 2020	[33] PAWR 2022
Technology	130-nm SiGe				130-nm SiGe	130-nm SiGe:C	28-nm Bulk CMOS	28-nm Bulk CMOS	45-nm CMOS SOI
Topology	Dif. 2-stage CE+CC with TRX SW				Dif. 2-stage CE+CE	Dif. 1-stage CC	Dif. 2-stage CS+CS	Dif. 2-stage CS+CS	1-stage 4-stacked-FET, Adaptive cap. & bias
BW_{3dB} [GHz]	22.2–32.0				19.0–29.5*	23.5–34.0	27.35–31.2	–	–
Frequency f_c [GHz]	24	26	28	30	28.5	28	30	28	25
Gain [dB]	30.0	30.0	29.3	28.1	20.0	19.4	15.7	18.5	17.6
P_{sat} [dBm]	20.8	20.7	20.6	20.0	17.0	22.7	14.0	18.9	21.5
oP_{1dB} [dBm]	19.0	19.1	18.6	16.9	15.2	22.1	13.2	18.5	–
PAE_{max} [%]	26.0	26.5	25.6	22.7	43.5	38.1	35.5	39.7	39.0
FoM	***92.6***	***93.3***	***92.9***	***91.2***	***82.5***	***86.9***	***74.7***	***82.3***	***83.2***
Active area [mm^2]	0.21				0.29	0.16	0.16	0.31	0.22
Modulation signal	64-QAM OFDM				64-QAM OFDM	64-QAM OFDM	64-QAM OFDM	64-QAM OFDM	–
EVM [dBc]	–25				–25	–25.2	–25	–25.4	–
Pout@EVM [dBm]	12.3				9.8	16.2	4.2	9.3	–

* Pout 1dB Bandwidth

** ITRS FoM = P_{sat} (dBm) + Gain (dB) + $10\log_{10}(\mathrm{PAE}_{\max}[\%]) + 20\log_{10}(f_c[\mathrm{GHz}])$ [37].

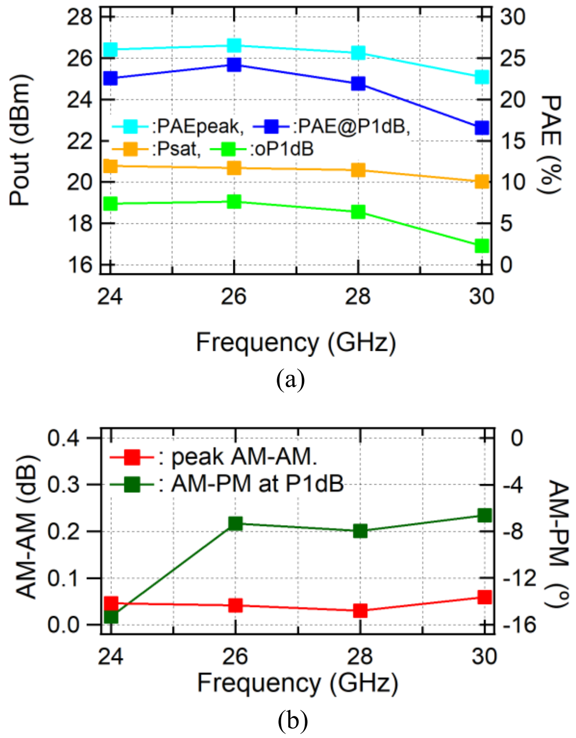

(a)

(b)

Fig. 13 Measured performances of the proposal PA at different frequencies. (a) Psat, oP1dB, PAE peak, and PAE at P1dB. (b) Peak AM-AM and AM-PM at P1dB.

and the peak AM-AM is 0.0 and 0.4 dB, respectively. Figure 13 summarizes the measured performance of the proposal PA, which is the counterpart of the simulated results shown in Fig. 7. The PA demonstrates Psat > 20 dBm from 24 to 30 GHz as expected from the load-pull simulations. Conversely, the loss of the OMN including TRX-SW is approximately 1 dB. The peak PAE of 30% expected by the load-pull simulation is calculated to drop to 24% as the output drops from 21 dBm to 20 dBm due to the loss of the OMN, which approximately matches the measured PAE peak. The measured AM-AM suppression agrees with the simulated AM-AM peak contour. The measured TX-mode oP1dB also shows good agreement with simulations.

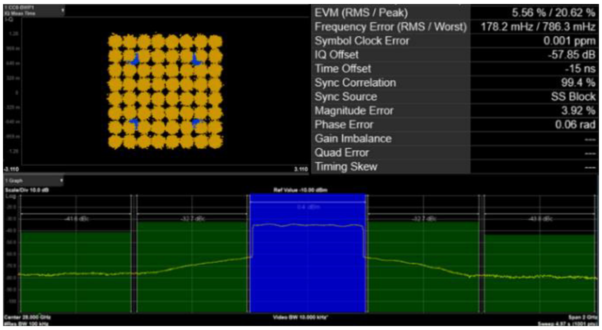
EVM (RMS / Peak) 5.56 % / 20.62 %
Frequency Error (RMS / Worst) 178.2 mHz / 786.3 mHz
Symbol Clock Error 0.001 ppm
IQ Offset -57.85 dB
Time Offset -15 ns
Sync Correlation 99.4 %
Sync Source SS Block
Magnitude Error 3.92 %
Phase Error 0.06 rad
Gain Imbalance ---
Quad Error ---
Timing Skew ---

Fig. 14 Measurement results of output spectrum and constellation using 64-QAM OFDM signals at 28 GHz with bandwidth of 400 MHz at EVM = –25 dB.

3.3 Modulated Signal Measurement

Figure 14 shows the measured output spectrum and constellation using 400-MHz 64-QAM OFDM signals at 28 GHz. The modulated input signal is generated by a Keysight VXG Signal Generator M9384B. The output from the PA is split in two: one to a Keysight UXA Signal Analyzer N9040B to measure the constellation and spectrum, and the other to a Keysight N8487A to monitor the output power. The average

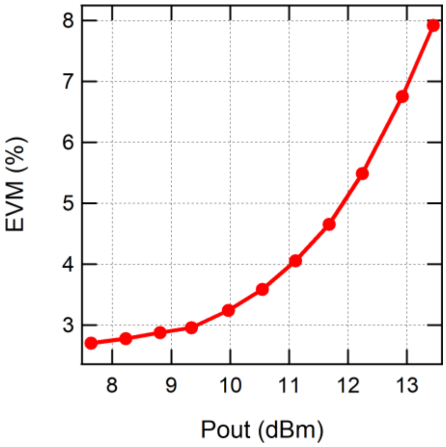

Fig. 15 Measurement results of EVM depending on Pout.

output power, modulation PAE, and ACPR are 12.3 dBm, 8.8%, and −32.7 dBc at −25 dB (5.6%) EVM, respectively. The EVM depending on Pout is shown in Fig. 15.

3.4 Comparison

Table 1 compares this work to recently reported PA ICs [27], [28], [31]–[33]. The ITRS FoM is included to compare the overall performance. It is noteworthy that even though the compared works do not contain any TRX switch or LNA, the proposal PA exhibits the highest ITRS FoM [37] of 92.9 at 28 GHz.

4. Conclusion

In this paper, we presented a linear wideband PA with low AM-AM distortion in 130-nm SiGe BiCMOS for 5G applications. The proposed PA achieves a Psat higher than 20 dBm with the PAE between 22% and 27% in a CW test over 24–30 GHz covering the 5G NR FR2 bands n257, n258 and n261. In a 64-QAM OFDM modulated signal test, the PA achieved the output power of 12.3 dBm with the modulation PAE of 8.8% at −25 dB EVM at 28 GHz. The achieved FoM (ITRS-defined) of 92.9 is higher than published state of the art PAs at similar frequencies.

References

[1] S. Suyama, J. Shen, A. Benjebbour, Y. Kishiyama, and Y. Okumura, “Super high bit rate radio access technologies for small cells using higher frequency bands,” Proc. IEEE MTT-S Int. Microw. Symp. (IMS), July 2014.

[2] T. Obara, T. Okuyama, Y. Aoki, S. Suyama, J. Lee, and Y. Okumura, “Indoor and outdoor experimental trials in 28-GHz band for 5G wireless communication systems,” Proc. IEEE PIMRC, pp.846–850, Aug. 2015.

[3] H. Murata, E. Okamoto, M. Mikami, A. Okazaki, S. Suyama, T. Inoue, J. Mashino, T. Yamamoto, and M. Taroumaru, “Radio access technologies for fifth generation mobile communications system: Review of recent research and developments in Japan,” IEICE Trans. Commun., vol.E99-B, no.8, pp.1638–1647, Aug. 2016.

[4] Y. Okumura, S. Suyama, J. Mashino, and K. Muraoka, “Recent activities of 5G experimental trials on massive MIMO technologies and 5G system trials toward new services creation,” IEICE Trans. Commun., vol.E102-B, no.8, pp.1352–1362, Aug. 2019.

[5] M. Sakai, K. Kamohara, H. Iura, H. Nishimoto, K. Ishioka, Y. Murata, M. Yamamoto, A. Okazaki, N. Nonaka, S. Suyama, J. Mashino, A. Okumura, and Y. Okumura, “Experimental field trials on MU-MIMO transmissions for high SHF wide-band massive MIMO in 5G,” IEEE Trans. Wireless Commun., vol.19, no.4, pp.2196–2207, April 2020.

[6] 3GPP, 5G NR specs, http://www.3gpp.org/DynaReport/38-series.htm

[7] Y. Azar, G.N. Wong, K. Wang, R. Mayzus, J.K. Schulz, H. Zhao, F. Gutierrez, D. Hwang, and T.S. Rappaport, “28 GHz propagation measurements for outdoor cellular communications using steerable beam antennas in New York city,” Proc. IEEE Int. Conf. on Communications (ICC), pp.5143–5147, June 2013.

[8] W. Roh, J.-Y. Seol, J. Park, B. Lee, J. Lee, Y. Kim, J. Cho, K. Cheun, and F. Aryanfar, “Millimeter-wave beamforming as an enabling technology for 5G cellular communications: Theoretical feasibility and prototype results,” IEEE Commun. Mag., vol.52, no.2, pp.106–113, Feb. 2014.

[9] Y. Suzuki, T. Kaho, K. Satoh, H. Okazaki, M. Arai, Y. Yamaguchi, S. Narahashi, and H. Shiba, “26 GHz band extremely low-profile front-end configuration employing integrated modules of patch antennas and SIW filters,” IEICE Trans. Electron., vol.E100-C, no.12, pp.1097–1107, Dec. 2017.

[10] B. Sadhu, Y. Tousi, J. Hallin, S. Sahl, S.K. Reynolds, Ö. Renström, K. Sjögren, O. Haapalahti, N. Mazor, B. Bokinge, G. Weibull, H. Bengtsson, A. Carlinger, E. Westesson, J.-E. Thillberg, L. Rexberg, M. Yeck, X. Gu, M. Ferriss, D. Liu, D. Friedman, and A. Valdes-Garcia, “A 28-GHz 32-element TRX phased-array IC with concurrent dual-polarized operation and orthogonal phase and gain control for 5G communications,” IEEE J. Solid-State Circuit, vol.52, no.12, pp.3373–3391, Dec. 2017.

[11] J.D. Dunworth, A. Homayoun, B.-H. Ku, Y.-C. Ou, K. Chakraborty, G. Liu, T. Segoria, J. Lerdworatawee, J.W. Park, H.-C. Park, H. Hedayati, D. Lu, P. Monat, K. Douglas, and V. Aparin, “A 28 GHz bulk-CMOS dual-polarization phased-array transceiver with 24 channels for 5G user and basestation equipment,” IEEE Int. Solid-State Circuits Conf. (ISSCC) Dig. Tech. Papers, pp.70–72, Feb. 2018.

[12] H.-T. Kim, B.-S. Park, S.-S. Song, T.-S. Moon, S.-H. Kim, J.-M. Kim, J.-Y. Chang, and Y.-C. Ho, “A 28-GHz CMOS direct conversion transceiver with packaged 2 × 4 antenna array for 5G cellular system,” IEEE J. Solid-State Circuits, vol.53, no.5, pp.1245–1259, May 2018.

[13] J. Dunworth, B.-H. Ku, Y.-C. Ou, D. Lu, P. Mouat, A. Homayoun, K. Chakraborty, A. Arnett, G. Liu, T. Segoria, J. Lerdworatawee, J.W. Park, H.-C. Park, H. Hedayati, A. Tassoudji, K. Douglas, and V. Aparin, “28 GHz phased array transceiver in 28nm bulk CMOS for 5G prototype user equipment and base stations,” IEEE MTT-S Int. Microw. Symp. Dig., pp.1330–1333, June 2018.

[14] K. Kibaroglu, M. Sayginer, T. Phelps, and G.M. Rebeiz, “A 64-element 28-GHz phased-array transceiver with 52-dBm EIRP and 8–12-Gb/s 5G link at 300 meters without any calibration,” IEEE Trans. Microw. Theory Techn., vol.66, no.12, pp.5796–5811, Dec. 2018.

[15] A. Nafe, M. Sayginer, K. Kibaroglu, and G.M. Rebeiz, “2 × 64 dual-polarized dual-beam single-aperture 28 GHz phased array with high cross-polarization rejection for 5G polarization MIMO,” IEEE MTT.-S Int. Microw. Symp. Dig., pp.484–487, June 2019.

[16] B. Sadhu, X. Gu, and A. Valdes-Garcia, “The more (antennas), the merrier: A survey of silicon-based mm-wave phased arrays using multi-IC scaling,” IEEE Microw. Mag., vol.20, no.12, pp.32–50, Dec. 2019.

[17] Y. Yin, Z. Zhang, T. Kanar, S. Zihir, and G.M. Rebeiz, “A 24–29.5

GHz 256-element 5G phased-array with 65.5 dBm peak EIRP and 256-QAM modulation," IEEE MTT-S Int. Microw. Symp. Dig., pp.687–690, Aug. 2020.

[18] H. Chung, Q. Ma, Y. Yin, L. Gao, and G.M. Rebeiz, "A 25–29 GHz 64-element dual-polarized/dual-beam small-cell with 45 dBm 400 MHz 5GNR operation and high spectral purity," IEEE MTT-S Int. Microw. Symp. Dig., pp.1267–1270, Aug. 2020.

[19] A. Khalil, I. Eshrah, A. Elsherief, A. Mehana, M. Abdalla, M. Mobarak, J. Kilpatrick, B. Hall, A. Ashry, H. Fahmy, S. Salim, R. Kernan, B. Herdeg, G. Sapia, M. El-Nozahi, M. Weheiba, M. D'Amato, C. Bautista, K. Chatzopoulos, A. Ghoniem, Y. Mosa, D. Roll, and K. Ok, "mm-wave 5G radios: Baseband to waves," IEEE Int. Solid-State Circuits Conf. (ISSCC) Dig. Tech. Papers, vol.64, pp.38–40, Feb. 2021.

[20] J. Pang, Z. Li, X. Luo, J. Alvin, R. Saengchan, A.A. Fadila, K. Yanagisawa, Y. Zhang, Z. Chen, Z. Huang, X. Gu, R. Wu, Y. Wang, D. You, B. Liu, Z. Sun, Y. Zhang, H. Huang, N. Oshima, K. Motoi, S. Hori, K. Kunihiro, T. Kaneko, A. Shirane, and K. Okada, "A CMOS dual-polarized phased-array beamformer utilizing cross-polarization leakage cancellation for 5G MIMO systems," IEEE J. Solid-State Circuits, vol.56, no.4, pp.1310–1326, April 2021.

[21] Q. Ma, H. Chung, Y. Yin, E. Wagner, B. Ustundag, K. Kibaroglu, M. Sayginer, and G. Rebeiz, "A 5G 25–29 GHz 64-element phased-array with 49–52 dBm EIRP, integrated up/down-converter and on-chip PLL," IEEE MTT-S Int. Microw. Symp. Dig., pp.854–857, June 2021.

[22] X. Gu, D. Liu, Y. Hasegawa, K. Masuko, C. Baks, Y. Suto, Y. Fujisaku, B. Sadhu, A. Paidimarri, N. Guan, and A. Valdes-Garcia, "Antenna-in-package integration for a wideband scalable 5G millimeter-wave phased-array module," IEEE Microw. Wirelss Compon. Lett., vol.31, no.6, pp.682–684, June 2021.

[23] Y. Hasegawa, M. Ota, T. Iwamura, Y. Nakatani, N. Oyaizu, K. Masuko, and N. Guan, "Compact and low-loss stripline bandpass filters made of liquid crystal polymer for n257 and n258 applications," Proc. European Microw. Conf. (EuMC), pp.437–440, April 2022.

[24] A. Paidimarri, M. Yoshiyama, J.-O. Plouchart, A. Valdes-Garcia, W. Lee, Y. Okuyama, M. Yeck, C. Ozdag, S. Chakraborty, Y. Yamaguchi, and B. Sadhu, "A high-linearity, 24–30 GHz RF, beamforming and frequency-conversion IC for scalable 5G phased arrays," Proc. IEEE Radio Freq. Integr. Circuits Symp. (RFIC), pp.103–106, June 2021.

[25] B. Sadhu, A. Paidimarri, W. Lee, M. Yeck, C. Ozdag, Y. Tojo, J.-O. Plouchart, X. Gu, Y. Uemichi, S. Chakraborty, Y. Yamaguchi, N. Guan, and A. Valdes-Garcia, "A 24-to-30 GHz 256-element dual-polarized 5G phased array with fast beam-switching support for >30,000 beams," Proc. IEEE Int. Solid-State Circuit Conf. (ISSCC), pp.436–438, Feb. 2022.

[26] B. Sadhu, A. Paidimarri, D. Liu, M. Yeck, C. Ozdag, Y. Tojo, W. Lee, K.X. Gu, J.-O. Plouchart, C.W. Baks, Y. Uemichi, S. Chakraborty, Y. Yamaguchi, N. Guan, and A. Valdes-Garcia, "A 24-30-GHz 256-element dual-polarized 5G phased array using fast on-chip beam calculators and magnetoelectric dipole antennas," IEEE J. Solid-State Circuits, vol.57, no.12, pp.3599–3616, Dec. 2022.

[27] T.-W. Li, M.-Y. Huang, and H. Wang, "A continuous-mode harmonically tuned 19-to-29.5GHz ultra-linear PA supporting 18Gb/s at 18.4% modulation PAE and 43.5% peak PAE," Proc. IEEE Int. Solid-State Circuit Conf. (ISSCC), pp.410–412, Feb. 2018.

[28] S. Shakib, H.-C. Park, J. Dunworth, V. Aparin, and K. Entesari, "A highly efficient and linear power amplifier for 28-GHz 5G phased array radios in 28-nm CMOS," IEEE J. Solid-State Circuits, vol.51, no.12, pp.3020–3036, Dec. 2016.

[29] K. Yamanaka, S. Shinjo, Y. Komatsuzaki, S. Sakata, K. Nakatani, and Y. Yamaguchi, "Overview and prospects of high power amplifier technology trend for 5G and beyond 5G base stations," IEICE Trans. Electron., vol.E104-C, no.10, pp.526–533, Oct. 2021.

[30] K. Nakatani, Y. Yamaguchi, T. Torii, and M. Tsuru, "A review of GaN MMIC power amplifier technologies for millimeter-wave applications," IEICE Trans. Electron., vol.E105-C, no.10, pp.433–440, Oct. 2022.

[31] T.-C. Tsai, C. Bohn, J. Hebeler, M. Kaynak, and A.Ç. Ulusoy, "A linear and efficient power amplifier supporting wideband 64-QAM for 5G applications from 26 to 30 GHz in SiGe:C BiCMOS," Proc. IEEE Radio Freq. Integr. Circuits Symp. (RFIC), pp.127–130, July 2021.

[32] Y.-W. Chang, T.-C. Tsai, J.-Y. Zhong, J.-H. Tsai, and T.-W. Huang, "A 28 GHz linear and efficient power amplifier supporting wideband OFDM for 5G in 28nm CMOS," IEEE/MTT-S Int. Microw. Symp. (IMS) Dig., pp.1093–1096, Aug. 2020.

[33] T. Sugiura and T. Yoshimasu, "25-GHz-band high efficiency stacked-FET power amplifier IC with adaptive controlled gate capacitor in 45-nm SOI CMOS," Proc. IEEE Topical Conf. on RF/Microw. Power Amplifiers Wireless Radio Appl. (PAWR), pp.26–28, Jan. 2022.

[34] R. Ishikawa, Y. Takayama, and K. Honjo, "Doherty amplifier design based on asymmetric configuration scheme," IEICE Trans. Electron., vol.E104-C, no.10, pp.496–505, Oct. 2021.

[35] R. Ishikawa, Y. Takayama, and K. Honjo, "A 4.5-GHz-band miniature outphasing GaN HEMT MMIC power amplifier," Proc. Asia-Pacific Microw. Conf. (APMC), Nov. 2021.

[36] C. Kamidaki, Y. Okuyama, T. Kubo, W. Lee, C. Ozdag, B. Sadhu, Y. Yamaguchi, and N. Guan, "A 24–30 GHz power amplifier with >20 dBm Psat and < 0.1 dB AM-AM distortion for 5G applications," Proc. Asia-Pacific Microw. Conf. (APMC), Nov. 2022.

[37] International Technology Roadmap for Semiconductors 2001, System Drivers Edition, p.10.

[38] A. Bevilacqua and A. Mazzanti, "Doubly-tuned transformer networks: A tutorial," IEEE Trans. Circuits Syst. II, Exp. Briefs, vol.68, no.2, pp.550–555, Feb. 2021.

[39] X. Bi, Y. Guo, and M. Je, "Analysis and design of gain enhanced cascode stage utilizing a new passive compensation network," IEEE Trans. Microw. Theory Techn., vol.61, no.8, pp.2892–2900, Aug. 2013.

Chihiro Kamidaki received the B.S. and M.S. degree in material science (physics) in Nagoya University in Aichi, Japan, in 2007 and 2009 respectively. He joined Fujikura Ltd. in 2010 and was involved in design and development of the cable and coil. From 2019, he has working on designing RF integrated circuits (RFICs) for communication systems. He is a member of the IEEJ and IEICE. He received the APMC Prize in the 2022 Asia Pacific Microwave Conference (APMC).

Yuma Okuyama received the B.S. and M.S. degrees from the Department of Physics, Tokyo Institute of Technology, Tokyo, Japan, in 2016 and 2018, respectively, for research on Surface physical properties. Since 2018, he has been with Fujikura Ltd., Chiba, Japan, working on the development of millimeter wave modules and ICs. He received the APMC Prize in the 2022 Asia Pacific Microwave Conference (APMC).

Tatsuo Kubo is a senior researcher in Fujikura Ltd., Sakura, Japan. He received the B.S. and M.S. degrees in mechanical engineering from Meiji University, Kanagawa, Japan, in 1999 and 2001. In 2001, he joined Oki Electric Industry Co., Ltd., Tokyo, Japan, where he was engaged in development on integrated circuits for optical communication. In 2006, he joined Fujikura Ltd. and was engaged in research and development on integrated circuits for optical communication. Since 2019, he has been working on millimeter-wave integrated circuits. He received the APMC Prize in the 2022 Asia Pacific Microwave Conference (APMC).

Wooram Lee received the B.Sc. and M.S. degrees in electrical engineering from the Korea Advanced Institute of Science and Technology (KAIST), South Korea, in 2001 and 2003, respectively, and the Ph.D. degree at Cornell University, Ithaca, NY, USA, in 2012. From 2015 to 2020, he was a Research Staff Member at the RF Circuits and Systems Group, IBM T.J. Watson Research Center, Yorktown Heights, NY, USA, where he was involved with the development of high-performance mm wave phased array circuits and systems and high-speed serial link transceivers for optical communication. He was also an Adjunct Assistant Professor at Columbia University, New York City, NY, USA, from 2017 to 2020. From 2012 to 2015, he was with Broadcom, San Jose, CA, USA, where he worked on multi-Gbps CMOS transceivers and data converters for broadband communication in optical, copper, and backplane applications. From 2003 to 2007, he was a Research Engineer at the Electronics and Telecommunications Research Institute (ETRI), Daejeon, South Korea, where he worked on optical transceivers and links. He is currently an Associate Professor at the Department of Electrical Engineering, Penn State University, PA, USA. His research interests are mm-wave and THz integrated circuits and systems for communication and sensing. Dr. Lee is a member of the Technical Program Committee of the IEEE BiCMOS and Compound Semiconductor Integrated Circuits and Technology Symposium (BCICTS) and the International Microwave Symposium (IMS). He received the Best Industry Paper Award (second place) from the IEEE Radio Frequency Integrated Circuits Symposium in 2019, the IEEE Solid-State Circuits Predoctoral Fellowship (the sole winner) for 2010–2011, and the Samsung Graduate Fellowship for 2007–2012. He was a recipient of the Best Paper Award at the IEEE Radar Conference in 2009, and a co-recipient of the IEEE Asia Pacific Microwave Conference (APMC) Prize in 2022.

Caglar Ozdag received the B.Sc. degree in EE from The University of British Columbia, Vancouver, BC, Canada, in 2012, and the M.Sc. degree in EE from Istanbul Technical University, Istanbul, Turkey, in 2015. In 2015, he joined Mikroelektronik Ltd., Istanbul, as an RFIC Design Engineer. From 2015 to 2017, he participated in the joint development of a 94-GHz phased array chipset with IBM Thomas J. Watson Research Center, Yorktown Heights, NY, USA. From 2017 to 2020, he held senior design roles at Mikroelektronik Ltd., working primarily on wide-band phased array transceivers. In 2020, he joined the RF Circuits and Systems Department, IBM Thomas J. Watson Research Center, working on state-of-the-art wireless and wireline communications systems. His research interests are millimeter-wave phased array circuits and systems for communications and sensing and high-speed serial link transceivers for optical communications. Mr. Ozdag is an Affiliate Member of the IEEE MTT-S Microwave and Millimeter-Wave Integrated Circuits Technical Committee. He received the APMC Prize in the 2022 Asia Pacific Microwave Conference (APMC). He is a member of the IEEE.

Bodhisatwa Sadhu received the B.E. degree in electrical and electronics engineering from the Birla Institute of Technology and Science Pilani (BITS Pilani), India, in 2007, and the Ph.D. degree in electrical engineering from the University of Minnesota, Minneapolis, MN, USA, in 2012. He was an Adjunct Assistant Professor at Columbia University, New York City, NY, USA, from 2017 to 2020. He is currently a Senior Research Scientist with the Communication Circuits and Systems Group, IBM T.J. Watson Research Center, Yorktown Heights, NY, USA. At IBM, he has led the design and demonstration of the world's first reported silicon-based 5G phased array IC, a low power 60-GHz CMOS transceiver IC for 802.11ad communications, a 256-element 5G phased array IC and module, a software-defined phased array radio, and several low phase noise frequency synthesizers. He has authored and coauthored more than 60 peer-reviewed papers, the book Cognitive Radio Receiver Front-Ends (Springer, 2014), and several book chapters. He also holds more than 70 issued U.S. patents. Dr. Sadhu was a recipient of the 2022 IEEE MTT-S Outstanding Young Engineer Award, the 2017 ISSCC Lewis Winner Award for Outstanding Paper (Best Paper Award), the 2017 IEEE Journal of Solid-State Circuits Best Paper Award, the 2017 Pat Goldberg Memorial Award for the Best Paper in computer science, electrical engineering, and mathematics published by IBM Research and co-recipient of the IEEE APMC prize in 2022. He received an IBM O-level Accomplishment Award for contributions to IBM P and Z mainframe processors, five IBM Outstanding Technical Achievement Awards, and was selected for the IBM Tech 2023 recognition for top technical contributors within IBM (among top ~2%). He stood 2nd in India in the Indian School Certificate (ISC) Examination in 2003, and won the BITS Pilani Silver Medal (2nd in class of more than 1000 students) in 2007. He was recognized as an IBM Master Inventor in 2017 and 2021 (three-year terms each) and selected by the National Academy of Engineering for its Frontiers of Engineering Symposium in 2020. He currently serves as an IEEE Distinguished Microwave Lecturer, an Associate Editor of IEEE Journal of Solid-State Circuits, Sub-Committee Chair and Steering Committee Member for IEEE RFIC Symposium, a TPC Member for IEEE ISSCC, and has served as a Guest Editor for IEEE Transactions on Microwave Theory and Techniques in 2021 and IEEE Journal of Solid-State Circuits in 2017. He is a senior member of the IEEE.

Yo Yamaguchi is a senior manager in Fujikura Ltd., Sakura, Japan. He received the B.S. and M.S. degrees in chemistry from Osaka University, Osaka, Japan, in 1989 and 1991, respectively. He received the D.E. degree in communication engineering from Tokyo Institute of Technology, Tokyo, Japan in 2010. In 1991, he joined NTT Radio Communication Systems Laboratories, Yokosuka, Japan, where he was engaged in research and development on MMICs. From 1999 to 2001, he was an Associate Manager at STE Telecommunication Engineering Co., Ltd., Tokyo, Japan, where he served as a Technical Consultant on wireless communications. From 2001 to 2019, he has been a Senior Research Engineer at NTT Network Innovation Laboratories, Yokosuka, Japan. From 2017 to 2019, he was a Visiting Professor at Kyushu University, Fukuoka, Japan. Since 2019, he joined Fujikura Ltd. and has been working on millimeter-wave integrated circuits. He received the Best Paper Award from the Institute of Electronics, Information and Communication Engineers (IEICE) Communication Society in 2011, from Electronics Society (ES) in 2014 and 2016, the IEICE ES Activity Testimonial from ES in 2017 and the APMC Prize in the 2022 Asia Pacific Microwave Conference (APMC). He served as a Technical Program Committee (TPC) member of the APMC 2006, and a TPC Vice Chair of the APMC 2010 and the APMC 2014. He also served as a secretary of the Institute of Electrical and Electronics Engineers (IEEE) Microwave Theory and Techniques Society Japan Chapter (MTT-S JC) Education Committee from 2009 to 2010, a secretary of the International Union of Radio Science Commission C (URSI-C) Japan national committee from 2011 to 2014, a secretary of the IEICE Technical Group on Microwave Engineering from 2014 to 2016, an associate editor of the IEICE Electronics Express from 2014 to 2017, a secretary of the IEEE MTT-S JC from 2016 to 2017, a director of IEICE ES Publication Activities Council from 2016 to 2018, a professional researcher of National Institute of Science and Technology Policy at Ministry of Education, Culture, Sports, Science and Technology in Japan from 2016 to 2019, and a committee member of the IEICE Japan National Committee of APMC from 2016 to 2020. Dr. Yamaguchi is a senior member of the IEEE and the IEICE.

Ning Guan received the B.E., M.E., and Ph.D. degrees in electrical and electronics engineering from Chiba University, Chiba, Japan, in 1985, 1987, and 1990, respectively. From 1991 to 2000, he was a Research Associate at the Department of Electronics and Mechanical Engineering, Chiba University, studying magnetostatic wave devices, the theory of propagation of electromagnetic waves, and applications of wavelet to boundary value problems in electromagnetic theory. Since 2000, he has been with Fujikura Ltd., Chiba, and has been working on the analysis and design of optical fibers and optical devices for telecommunications, microwave devices, and antennas for mobile communications. His current research interests are in the design and development of millimeter-wave components and phased array antenna modules for 5G applications. He received the APMC Prize in the 2022 Asia Pacific Microwave Conference (APMC). He is a senior member of the IEEE.